Heat Transfer Research 46(6), 541–562 (2015)

EFFECTS OF BLOCKAGE RATIO AND PRANDTL NUMBER ON STEADY FLOW AND HEAT TRANSFER AROUND AN INCLINED SQUARE CYLINDER

Jaber Aboueian-Jahromi, Alireza Hossein Nezhad,* & Amin Behzadmehr

Department of Mechanical Engineering, University of Sistan and Baluchestan, Zahedan, Iran

*Address all correspondence to Alireza Hossein Nezhad
E-mail: Nezhadd@hamoon.usb.ac.ir

Numerical investigation of flow and heat transfer around a long heated inclined square cylinder placed in a horizontal plane channel in a steady laminar regime is carried out for the conditions: $1 \le Re \le 40$, $0.7 \le Pr \le 100$, inclination angle equal to 45° and blockage ratio to $\beta = 1/8$, 1/6, and 1/4. The streamlines and isotherms are presented to elucidate the effects of the channel confinement, Prandtl number, and two thermal boundary conditions (constant wall temperature, CWT, and uniform heat flux, UHF) on the physics of the problem. Generally, an increase in a blockage ratio increases the drag coefficient and decreases the wake length. The average Nusselt number also increases with Prandtl and/or Reynolds number. Furthermore, decreasing the blockage ratio decreases the dimensionless local pressure drop and increases the average Nusselt number for low Re and Pr numbers. This can be an economical result for improving the thermal efficiency of the problem. However, for larger Reynolds and Prandtl numbers the average Nusselt number and local pressure drop increase with the blockage ratio. Finally, some simple correlations are introduced for recirculation length, drag coefficient, dimensionless local pressure drop, and average Nusselt number at different blockage ratios.

KEY WORDS: *inclined square cylinder, bluff body, steady channel flow, blockage ratio, local pressure drop, Nusselt number*

1. INTRODUCTION

The study of flow and heat transfer around cylindrical bluff bodies of different cross sections is a classical problem and thus has been the subject of intense experimental and numerical investigations for a long time. The importance of these flows in numerous industrial applications such as electronic cooling, cooling towers, gas and oil pipelines, flow meters, chimneys, antennas, support structures, heat exchangers, etc. also adds interest to this problem. There are some thorough reviews on the flow and heat transfer around the most commonly studied shapes, i.e., circular (Zdravkovich,

1064-2285/15/$35.00 © 2015 by Begell House, Inc.

NOMENCLATURE

A^*	side of the square cylinder (= A/b)
b	diameter of the square cylinder, m
C_d	total drag coefficient (= $2F_d/\rho U_{max}^2 b$)
c_p	specific heat of the fluid, $J \cdot kg^{-1} \cdot K^{-1}$
F_d	drag force on the cylinder, $N \cdot m^{-1}$
h	local heat transfer coefficient, $W \cdot m^{-2} \cdot K^{-1}$
$\overline{h}$	average heat transfer coefficient, $W \cdot m^{-2} \cdot K^{-1}$
j	Colburn j factor (= Nu/(Re $Pr^{1/3}$))
k	thermal conductivity, $W \cdot m^{-1} \cdot K^{-1}$
L_1	height of the computational domain, m
L_2	length of the computational domain, m
L_r^*	recirculation length (= L_r/b)
n_s^*	normal direction to the cylinder surface
Nu_l	local Nusselt number (= hb/k)
Nu	average Nusselt number (= hb/k)
p^*	pressure (= $p/(\rho U_{max}^2)$)
ΔP_{cyl}^*	cylinder pressure drop (= $\Delta P_{cyl}/(\rho U_{max}^2)$)
Pr	Prandtl number (= $\mu c_p/k$)
q_w	local heat flux, $W \cdot m^{-2}$
q_{ave}	average heat flux, $W \cdot m^{-2}$
Re	Reynolds number (= $\rho U_{max} b/\mu$)
s^*	cylinder surface area (= s/b)
T^*	temperature (= $(T - T_{in})/(T_w - T_{in})$ for CWT or $(T - T_{in})/(q_w b/k)$ for UHF)
u^*	x-component of velocity (= u/U_{max})
U_{max}	maximum velocity at the channel inlet, $m \cdot s^{-1}$
v^*	y-component of velocity (= v/U_{max})
x^*	streamwise coordinate (= x/b)
X_d^*	downstream distance of cylinder (= X_d/b)
X_u^*	upstream distance of cylinder (= X_u/b)
y^*	transverse coordinate (= y/b)
Greek symbols	
α	inclination angle of cylinder
β	blockage ratio (= b/L_1)
δ	finest grid size, m
Δ	coarsest grid size, m
μ	dynamic viscosity of fluid, $kg\ m^{-1} \cdot s^{-1}$
ρ	density of fluid, $kg \cdot m^{-3}$
Acronyms	
CWT	constant wall temperature
UHF	uniform heat flux
Subscripts	
in	inlet condition
w	wall surface of the inclined square cylinder
Superscript	
*	dimensionless variable

1997, 2003; Ahmad, 1996) and square (Dhiman et al., 2005, 2006; Sharma and Eswaran, 2004) cylinders in the pertinent literatures. Here, only prominent points and subsequent studies are detailed with a special reference to the effects of the blockage ratio (β) on the flow and heat transfer characteristics around square cylinders. The blockage ratio here is the diameter of a square cylinder projected to the height of the channel. Davis et al. (1984) presented both numerical and experimental results for confined flow around rectangular cylinders for two blockage ratios (β = 1/4 and 1/6) at $100 \leq Re \leq 1850$. They found that the presence of confining walls and the form of the upstream velocity profile lead to numerous changes in the characteristics of the flow around rectangles. Breuer et al. (2000) conducted a two-dimensional study for a confined flow around a square cylinder mounted inside a plane channel with β = 1/8 by two numerical techniques, namely, a lattice-Boltzmann automata and a finite volume method in the Reynolds number range $0.5 \leq Re \leq 300$ with a parabolic velocity profile at the channel inlet. They evaluated the integral quantities such as the drag coefficient, recirculation length, and the Strouhal number for both steady ($0.5 \leq Re \leq 60$) and unsteady ($60 \leq Re \leq 300$) flows. Turki et al. (2003) numerically studied the forced and mixed convection around a heated square cylinder mounted inside a horizontal channel for a two-dimensional unsteady flow region $62 \leq Re \leq 200$ at the Richardson numbers up to 0.1 for two blockage ratios of 1/4 and 1/8. They concluded that for pure forced convection the value of the critical Reynolds number (onset of periodic flow) increases with an increasing blockage ratio. They also proposed some correlations for the Nusselt number. Gupta et al. (2003) studied the heat transfer of non-Newtonian power-law fluids around a confined square cylinder for $5 \leq Re \leq 40$, $1 \leq Pr \leq 10$ ($5 \leq Pe = RePr \leq 400$) and the power-law index between 0.5 and 1.4 for both CWT and UHF conditions on the surface of the cylinder for β = 1/8. Dhiman et al. (2005) also studied the effects of blockage ratio (β = 1/8, 1/6, and 1/4) and Prandtl number ($0.7 \leq Pr \leq 4000$) on the characteristics of cross flow and heat transfer of Newtonian fluids around a confined square cylinder with no inclination angle in a steady flow regime ($1 \leq Re \leq 45$).

In comparison with circular cylinders, rectangular cylinders introduce the dependence of the orientation to the flow as an additional parameter. It is quite likely that the flow characteristics, aerodynamic forces, vortex shedding frequency, heat-transfer performance, etc. will exhibit distinct behaviors in different ranges of incidence for square cylinders (Igarashi, 1984). However, still much less is known about the momentum and heat transfer characteristics of flow over a square cylinder with an inclination angle. Sohankar et al. (1998) studied the onset of vortex shedding and the effects of the blockage ratios on unsteady flow of Newtonian fluids over a square cylinder at incidence ($0^o \leq \alpha \leq 45^o$) in a 2D channel with frictionless walls for $45 \leq Re \leq 200$ (Re based on the uniform entrance velocity and the projected diameter of the square). They concluded that the changes in the locations of the flow separation points due to the variations in the inclination angle of the square cylinder might result in drastic changes of the key flow parameters such as the force coefficients and Strouhal number. They also obtained the critical Reynolds number of Re = 42 for the onset of vortex shedding at $\beta = 0.05$ and $\alpha = 45^{o}$. They also conjectured that the critical Reynolds number increases with an increasing blockage ratio. Yoon et al. (2010) also carried out a parametric numerical study to investigate the effect of inclination angle on the flow topology and flow-induced forces on an unconfined inclined square cylinder in both steady and unsteady flow regimes. They showed that the critical Reynolds number for the onset of vortex shedding is minimum at $\alpha = 45^{o}$ (Re= 39). They also obtained a correlation between the critical Reynolds number and the growth rate of the recirculation length for unconfined cylinders regardless of the shape of the bluff body. Chakrabarty and Brahma (2007) also carried out experiments to investigate the unsteady flow and heat transfer of air around a heated square cylinder in a wind tunnel for different blockage ratios and angles of attack of the cylinder at $Re = 4.9 \cdot 10^4$. In a recent work, Aboueian-Jahromi et al. (2011) studied the effects of the inclination angle of a confined square cylinder on the steady flow and heat transfer of non-Newtonian power-law fluids. They defined a local pumping power and showed that a decrease in the power-law index or an increase in the inclination angle decrease this local pumping power and increase the average Nusselt number. Moreover, an inclined square cylinder in channel flows can be an effective tool to control heat transfer from the channel walls (Valencia, 1995). The maximum heat transfer to the channel walls also occurs for a cylinder at an angle of attack of 45^{o} (Yoon et al., 2009). Recently, some works have been done on channel flows with different obstacles using the lattice Boltzmann method (Benim et al., 2011; Moussaoui et al., 2010, etc.). Moussaoui et al. (2010) simulated two-dimensional incompressible flow and heat transfer in a horizontal channel differentially heated and obstructed by an inclined square cylinder with an inclination angle of 45^{o} for $0 \leq Re \leq 300$, Pr = 0.71, and $\beta = 1/4$. They used a strategy based on the lattice Boltzmann method for the fluid velocity field and finite difference for the temperature field. They imposed a fully developed velocity profile at the inlet and the Neumann boundary condition at the outlet of the channel. They found the critical Reynolds number (based on the square diameter and the maximum inlet velocity) for the onset of vortex shedding to be about 82.

Most of the scant available literatures on the fluid flow over an inclined square cylinder are in an unsteady region surveying the vortex-shedding phenomenon. On the other hand, much less attention has been devoted to heat transfer characteristics. The studies of the effects of the Prandtl number on heat transfer have not been of interest to scientists over the years. However, it is readily admitted that in chemical, petroleum, and oil-related industrial applications the values of the Prandtl number of up to 100 are frequently encountered for steady flows of process streams (owing to their high viscosities). Furthermore, Sohankar et al. (1998) found that flow around a square cylinder with $\alpha = 45^{o}$ is steady up to about the critical Re = 42. Increasing the blockage ratio also increases this critical Re number. Therefore, as our aim is to study the steady flow, the present work is limited to a maximum Reynolds number of 45. Recently, little prior work (Dhiman et al., 2005, 2006; Bharti et al., 2007; Sahu et al., 2009) are carried out on the effect of Prandtl number on the forced convection heat transfer from cylinders of circular or square (with no angle of attack) cross section for Newtonian liquids. However, there is no numerical result in the literature on the effects of Prandtl number on the heat transfer coefficients around an inclined square cylinder at different blockage ratios. Therefore, the main purpose of the present work is to study the effects of Prandtl numbers ($0.7 \leq \mathrm{Pr} \leq 100$) and the wall confinement (β = 1/8, 1/6, and 1/4) on steady flow and heat transfer around an inclined square cylinder at an incidence angle of $\alpha = 45^{\mathrm{o}}$ and $1 \leq \mathrm{Re} \leq 40$ for two thermal boundary conditions (CWT and UHF).

2. PROBLEM STATEMENT AND GOVERNING EQUATIONS

The problem of interest here is steady, incompressible, two-dimensional laminar flow of Newtonian fluids passing over a square cylinder (diameter = b) at an angle of 45^{o} with respect to the channel centerline. The cylinder is symmetrically confined in a channel with adiabatic walls (Fig. 1). Two different thermal boundary conditions, CWT and UHF, on the square cylinder surfaces are considered here. The aim is the simulation of an infinitely long channel. However, as the computational domain has to be finite, a parabolic velocity profile (fully developed assumption) with a maximum value of U_{max} and a constant temperature of T_{in} is used at the inlet of the channel and the Neumann boundary condition is imposed at the channel outlet. The thermo-physical properties of the fluid are assumed independent of temperature and the viscous dissipation effects are neglected. These two assumptions restrict the applicability of the results to the situations where the maximum temperature difference and the Brinkman number in the flow domain remain low enough in order to satisfy the temperature independency and viscous dissipation negligibility, respectively. The Brinkman number provides an adequate estimate of the ratio between the heat generated by viscous heating and the heat exchanged at the wall (Coelho and Pinho, 2009). Three different

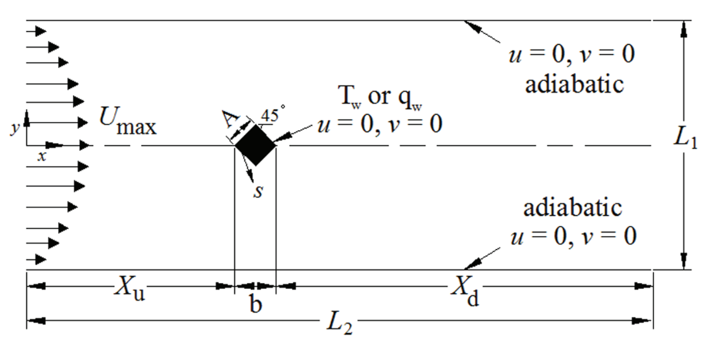

FIG. 1: Schematic of a confined flow over an inclined square cylinder

blockage ratios ($\beta = 1/8$, 1/6, and 1/4) are also used in this work. The blockage ratio varies with L_1 for a fixed b.

The dimensional governing equations in conjugation with the pertinent boundary conditions are solved numerically to obtain velocity, pressure, and temperature fields (Fig. 1). However, the dimensionless forms of the governing equations and boundary conditions are written as follows to obtain the effective dimensionless numbers in the problem:

continuity

$$\frac{\partial u^*}{\partial x^*} + \frac{\partial v^*}{\partial y^*} = 0\,, \tag{1}$$

x-momentum

$$u^* \frac{\partial u^*}{\partial x^*} + v^* \frac{\partial u^*}{\partial y^*} = -\frac{\partial p^*}{\partial x^*} + \frac{1}{\mathrm{Re}}\left[\frac{\partial^2 u^*}{\partial x^{*2}} + \frac{\partial^2 u^*}{\partial y^{*2}}\right], \tag{2}$$

y-momentum

$$u^* \frac{\partial v^*}{\partial x^*} + v^* \frac{\partial v^*}{\partial y^*} = -\frac{\partial p^*}{\partial y^*} + \frac{1}{\mathrm{Re}}\left[\frac{\partial^2 v^*}{\partial x^{*2}} + \frac{\partial^2 v^*}{\partial y^{*2}}\right], \tag{3}$$

energy equation

$$u^* \frac{\partial T^*}{\partial x^*} + v^* \frac{\partial T^*}{\partial y^*} = \frac{1}{\mathrm{Re}\cdot \mathrm{Pr}}\left(\frac{\partial^2 T^*}{\partial x^{*2}} + \frac{\partial^2 T^*}{\partial y^{*2}}\right). \tag{4}$$

The symbol * represents a nondimensional quantity. All the physical variables are nondimensionalized using the diameter of the cylinder (b), the maximum velocity at the channel inlet (U_{max}), and the maximum dynamic pressure at the channel inlet (ρU_{max}^2) as scaling variables for the length, velocity, and pressure, respectively. The dimensionless temperature is defined as $(T - T_{\mathrm{in}})/(T_{\mathrm{w}} - T_{\mathrm{in}})$ and $(T - T_{\mathrm{in}})/(q_{\mathrm{w}}b/k)$ for the CWT and UHF boundary conditions, respectively. The two dimensionless groups Re and Pr denote the Reynolds and Prandtl numbers, respectively and are defined as

$$\mathrm{Re} = \frac{\rho\, U_{\mathrm{max}}\, b}{\mu}\,, \tag{5}$$

$$\mathrm{Pr} = \frac{\mu\, C_{\mathrm{p}}}{k}\,. \tag{6}$$

The boundary conditions for the momentum and energy equations in their dimensionless forms may be written as given below (Fig. 1)

- At the channel inlet, flow is assumed to be fully developed with a constant temperature:

$$u^* = 1 - \left|2\beta y^*\right|^2 , \ v^* = 0, \ T^* = 0 ,$$

where $-L_1/2b \le y^* \le L_1/2b$.

- At the upper and lower walls, the usual no-slip condition for flow and adiabatic condition for energy are

$$u^* = 0, \ v^* = 0, \ \frac{\partial T^*}{\partial y^*} = 0.$$

- At the wall surface of the square cylinder, the no-slip boundary condition with two thermal boundary conditions (CWT and UHF) are used:

$$u^* = 0, \ v^* = 0, \ T^* = 1 \text{ (CWT)} \ \text{ or } \ \frac{\partial T^*}{\partial n_s^*} = -1 \ \text{ (UHF)},$$

  where n_s^* is the dimensionless normal distance to the surface of the cylinder.
- At the channel outlet, homogenous Neumann boundary conditions for velocity and temperature are used:

$$\frac{\partial u^*}{\partial x^*} = 0, \ \frac{\partial v^*}{\partial x^*} = 0, \ \frac{\partial T^*}{\partial x^*} = 0.$$

Some important parameters used in the following sections are also defined as, for example, the total drag coefficient:

$$C_d = \frac{2F_d}{\rho b U_{max}^{\ 2}} = 2\int_s (\sigma^{(n)^*} \cdot \mathbf{i})\, ds^*, \tag{7}$$

where F_d, $\sigma^{(n)^*}$, **i,** and s^* are the total drag force, the nondimensional stress vector in plane **n**, the unit vector of the x coordinate axis, and the nondimensional surface area, respectively.

As in the authors' previous work (Aboueian-Jahromi et al., 2011), the nondimensional local pressure drop for the cylinder is defined as follows:

$$\Delta P^*_{cyl.} = \Delta P^*_{cc.} - \Delta P^*_{ch.} \tag{8}$$

where $\Delta P^*_{cc.}$ and $\Delta P^*_{ch.}$ are the difference between the nondimensional static pressures at the inlet and outlet of the channel with and without a cylinder, respectively. The following relationship is also derived analytically for $\Delta P_{ch.}$ (Chhabra and Richardson, 2008):

$$\Delta P_{ch.} = \frac{8\mu\, U_{max} L_{ch.}}{H^2}\,. \tag{9}$$

The local Nusselt number for the CWT boundary condition is

$$Nu_l = \frac{hb}{k} = -\frac{\partial T^*}{\partial n_s^*}\,. \tag{10}$$

The local Nusselt number for the UHF boundary condition is

$$\mathrm{Nu}_l = \frac{hb}{k} = \frac{1}{T_w^*}\,. \tag{11}$$

Such local values are further averaged on the surface of the cylinder to obtain the average Nusselt number of the square cylinder as follows:

$$\mathrm{Nu} = \frac{\bar{h}b}{k} = \frac{1}{4A^*}\int_s \mathrm{Nu}_l ds^*, \tag{12}$$

where A^* is the dimensionless side of the square cylinder. Therefore, the total heat flux on the surface of the cylinder, q_{tot}, for CWT can be calculated as

$$q_{tot} = 4A\bar{h}\left(T_w - T_{in}\right). \tag{13}$$

3. NUMERICAL METHOD

A finite volume method was adapted to the staggered grids to solve the governing equations subjected to the aforementioned boundary conditions. The grid structure used in the present work is shown for the entire computational domain in Fig. 2. It consists of separate zones with uniform and nonuniform grid distribution having fine grids in the regions of large gradients and coarser grids in the regions of low gradients. There are three different grid distributions along the centerline of the channel in the x^* direction. The finest grid with a cell size δ is used uniformly in an inner region around the obstacle over a distance of 1.5b to capture wake–wall interactions in both directions. The coarsest uniform grid distribution in the x^* direction with a constant

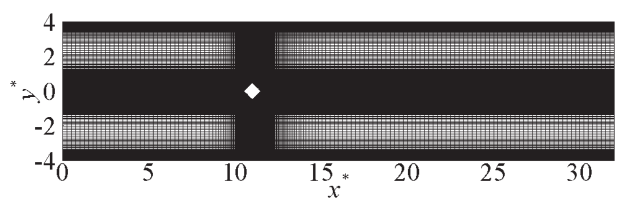

FIG. 2: Computational grid structure

cell size, $\Delta = 0.25b$, is applied in the outer region that extends $8.5b$ from the inlet and $16.5b$ from the outlet surface of the channel. A scheme with a constant ratio of any two succeeding interval lengths has been used for stretching the cell sizes between these limits of δ and Δ in the x^* direction. A similar scheme is employed symmetrically for generating the grid points in the region $0.25b$ away from the side corners of the cylinder to the channel walls in the y^* direction. A fine grid size δ is also clustered near the upper and lower walls of the channel. The semi-implicit method for the pressure-linked equations (SIMPLE algorithm) was applied for pressure–velocity decoupling. A second-order upwind scheme was employed to discretize the convective terms in the momentum and thermal energy equations while the diffusive terms were discretized using central differences. The velocity fields obtained by solving the Navier–Stokes equations were used as an input to the thermal energy equation to calculate the temperature field. Furthermore, the accuracy and reliability of the numerical results are dependent on the choices of an optimal grid and upstream and downstream distances describing the flow domain. For both domain and grid independence, computations have been carried out for the two extreme values of the Reynolds number (Re = 1 and 40) each for the two extreme values of Prandtl number (Pr = 1 and 100) for both thermal boundary conditions at the smallest blockage ratio $\beta = 1/8$. Increasing the upstream extent from 8.5 and 10.5 to 13.5 (for $X_d^* = 20.5$) produces the maximum percentage changes of 0.07% and 0.02% in C_d for Re = 40, and 0.18% and 0.05% in Nu for Re = 1, Pr = 1. Furthermore, increases in the downstream distance from 4.5, 6.5 and 10.5 to 20.5 (for $X_u^* = 10.5$) also produce the maximum percentage changes of 0.88%, 0.24%, and 0.006% in C_d and 0.16%, 0.04%, and 0.001% in Nu for Re = 40, Pr = 1, respectively. In addition, an increase from $X_d^* = 20.5$ to 30 has no significant effects on the global flow and heat transfer quantities (less than 0.01%). Therefore, the nondimensional upstream and downstream distances of the computational domain are selected $X_u^* = 10.5$ and $X_d^* = 20.5$, respectively. However, because of the influence of the shear stress on the channel walls in the definition of the dimensionless local pressure drop [Eq. (8)], a larger downstream distance is needed for this parameter. Figure 3 shows the effects of X_d^* (X_d^* = 21, 42, 63, 84, and 105) on $\Delta P^*_{\mathrm{cyl.}}$ for three different blockage ratios at Re = 40. This figure shows that the increases in X_d^* from 84 to 105 for $\beta = 1/8$, from 63 to 84 for $\beta = 1/6$, and from 42 to 63 for $\beta = 1/4$ lead to small variations in $\Delta P^*_{\mathrm{cyl.}}$. Therefore, in this research the $\Delta P^*_{\mathrm{cyl.}}$ results are presented with X_d^* = 84, 63, and 42 for β = 1/8, 1/6, and 1/4, respectively. This study also implies the needs of the larger downstream distance for smaller blockage ratios.

For grid independence studies, it was seen that the maximum changes in C_d and Nu mostly occurred for Re = 40 and Pr = 100. Table 1 shows the effects of six different grid structures on C_d and Nu. The refinement in the grid from G5 to G6 shows 0.06%, 0.05%, and 0.49% changes for C_d, Nu (for Pr = 1), and Nu (for Pr = 100), respectively. Therefore the grid G5 (314×329 and $\delta = 0.01$) is believed to be sufficiently refined to simulate flow and heat transfer phenomena.

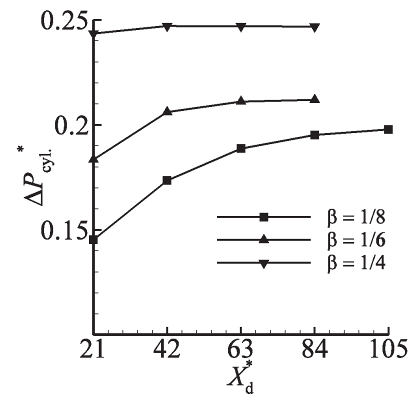

FIG. 3: Effects of X_d^* on $\Delta P_{cyl.}^*$ for different blockage ratios at Re = 40

TABLE 1: Grid independence study of C_d and Nu for Re = 40 (CWT) and β = 1/8

Grid	δ	Grid size ($M \times N$)	No. of cells	C_d	Nu (Pr = 1)	Nu (Pr = 100)
G1	0.03	136 × 205	28,404	1.5906	3.7252	20.8033
G2	0.02	186 × 241	45,538	1.5962	3.7159	19.9335
G3	0.01	186 × 241	50,310	1.6028	3.7074	19.2426
G4	0.01	250 × 335	87,826	1.6028	3.7077	19.2140
G5	0.01	314 × 329	107,390	1.6032	3.7085	19.2216
G6	0.008	292 × 380	117,504	1.6042	3.7068	19.1280

Note: M and N are the numbers of cells on the entrance line and walls of the channel, respectively; δ is the grid spacing on the cylinder surface.

4. RESULTS AND DISCUSSION

The numerical computations have been carried out for the following dimensionless parameters: Reynolds number, Re = 1, 2, and 5 to 40 in steps of 5; Prandtl number, Pr = 0.7, 1, 10, 50, and 100, and blockage ratio β = 1/8, 1/6, and 1/4. The effects of two classical thermal boundary conditions, i.e., CWT and UHF, have also been investigated for the above ranges of conditions.

4.1 Validation of Results

In order to assess the accuracy of the obtained results for the inclined square cylinder, the numerical investigation of flow and heat transfer around a square cylinder with no angle of incidence ($\alpha = 0^o$) are also carried out and the results are compared with the existing works (Dhiman et al., 2005; Breuer et al., 2000). In Fig. 4a, the to-

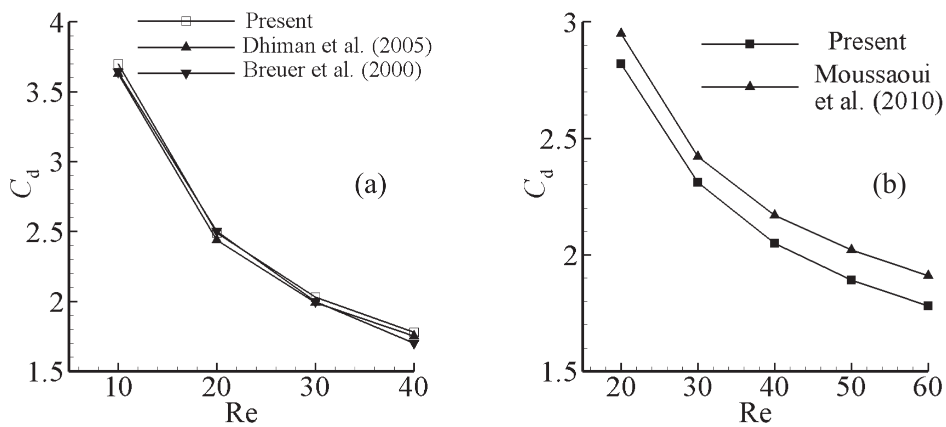

FIG. 4: Comparisons with previous works: (a) $\alpha = 0^o$ and $\beta = 1/8$, (b) $\alpha = 45$ and $\beta = 1/4$

tal drag coefficient (C_d) is obtained and compared with the results given by Dhiman et al. (2005) and Breuer et al. (2000) for a confined flow around a square cylinder ($\alpha = 0^o$, $\beta = 1/8$) for Re = 10, 20, 30, and 40. In both of these works, the finite volume method with 100 control volumes on each face of the cylinder is used. The maximum deviations between the present C_d and those of Dhiman et al. (2005) and Breuer et al. (2000) in Fig. 4a amount to about 2% and 4.5%, respectively. Furthermore, for evaluating the obtained heat transfer characteristics, a comparison of the present average Nusselt number with those of Dhiman et al. (2005) is presented in Table 2. A good agreement is seen to exist between the present Nusselt numbers and those of Dhiman et al. (2005) with a maximum deviation of about 1.6%.

On the other hand, for validating the results within the desired inclination angle, a comparison of the C_d with the results of Moussaoui et al. (2010) is made in Fig. 4b for an inclined square cylinder ($\alpha = 45^o$) with $\beta = 1/4$ for Re = 20, 30, 40, 50, and 60. The maximum deviation of about 7.3% is seen in Fig. 4b between the results. Of course, a main part of this deviation is related to the differences in the finite volume method and the lattice Boltzmann equation used by Moussaoui et al. (2010) to obtain the velocity field. The nondimensional wake lengths are also exactly similar to the values reported by Dhiman et al. (2005) for all Reynolds numbers studied here. Gen-

TABLE 2: Comparison of the present Nu number with Dhiman et al.'s (2005) results ($\alpha = 0$, $\beta = 1/8$)

	Re = 10		**Re = 20**		**Re = 30**		**Re = 40**	
Pr	**10**	**100**	**10**	**100**	**10**	**100**	**10**	**100**
Present	3.67	7.58	4.82	10.37	5.75	12.53	6.53	14.28
Dhiman et al. (2005)	3.66	7.64	4.88	10.41	5.69	12.52	6.59	14.15

erally, the normal deviations between the numerical results depend on the different grid structures, solution algorithms, and other numerical errors.

4.2 Flow Patterns

Figure 5 shows streamlines around the inclined square cylinder for Re = 1, 20, and 40 and β = 1/8, 1/6, and 1/4. As viscous forces dominate the flow at low Reynolds numbers, steady flow with no separation points is clearly seen in Fig. 5 at Re = 1 for all blockage ratios.

As the Reynolds number is increased for a fixed blockage ratio, the flow separation occurs on the side corners of the squared cylinder, and two small symmetric vortices, rotating in opposite directions, are observed in the recently created wake region behind the obstacle. The sizes of these vortices increase with increasing Reynolds number or decreasing blockage ratio. In the next section, the recirculation length is formulated based on Re for different blockage ratios.

4.3 Recirculation Length

Figure 6a shows the nondimensional recirculation length, L_r^* (= L_r/b), as a function of the Reynolds number for different blockage ratios. The recirculation length (L_r) is measured as the distance from the rear corner of the cylinder to the point of reattachment for the near closed streamline (u = 0, v = 0) on the line y = 0 in the downstream section. Since the head loss increases with the blockage ratio in the channel, the length of the recirculation region is seen to decrease with a rise in the blockage ratio.

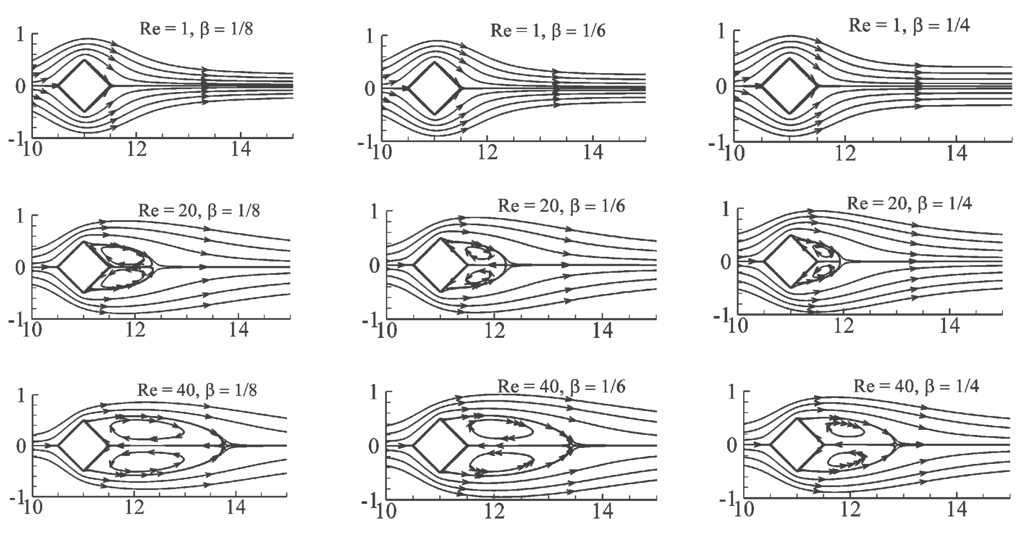

FIG. 5: Streamlines for Re = 1, Re = 20, and Re = 40 at different blockage ratios

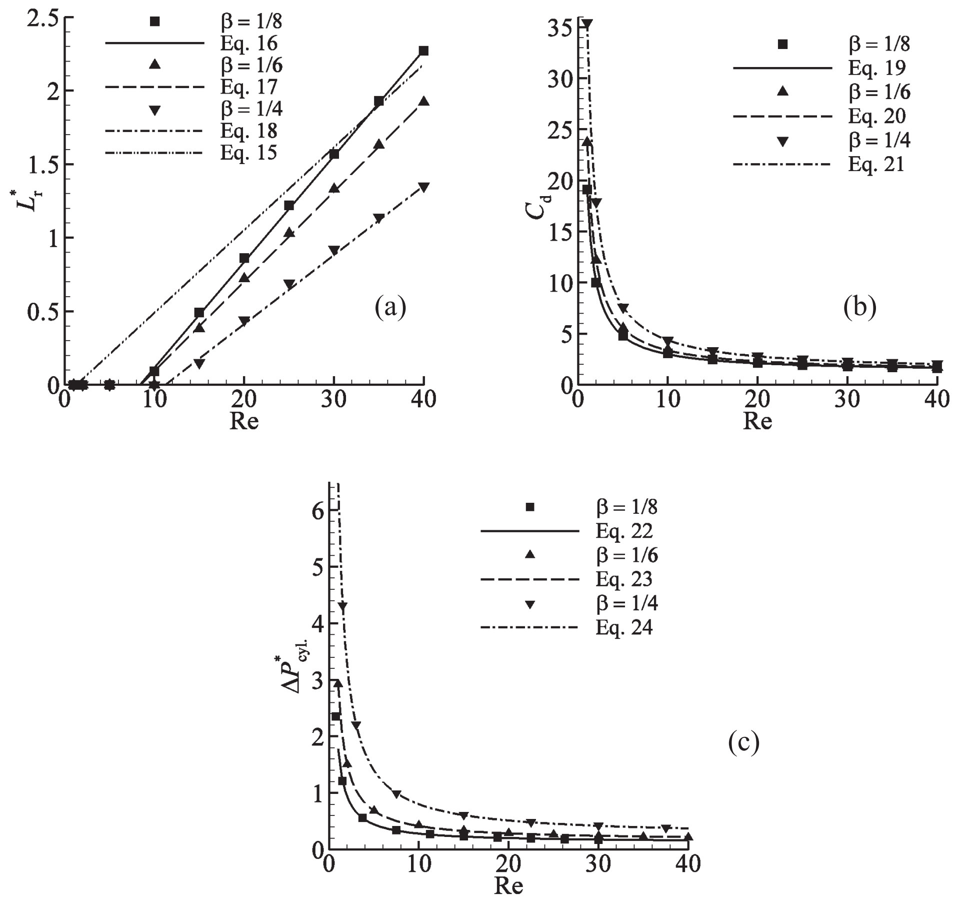

FIG. 6: Variations of L_r^* (a), C_d (b), and $\Delta P^*_{cyl.}$ (c) with Re for different β

However, since an increase in Re diminishes the importance of viscous forces, the recirculation length increases with Re for a fixed blockage ratio. This increase is completely linear for β = 1/8 and 1/6, but a quite small nonlinearity is observed for β = 1/4. Zdravkovich (1997) suggested a linear empirical relation for the recirculation length of an unconfined circular cylinder as

$$L_r^* = 0.05\ \mathrm{Re}\,. \tag{14}$$

For 4.4 ≤ Re ≤ 40 Dhiman et al. (2005) also proposed linear relationships between the recirculation length and Reynolds number for a square cylinder with no inclination angle for three different blockage ratios. The following is one of these relationships for β = 1/8 in a steady flow regime:

$$\text{For } 5 \le \mathrm{Re} \le 45\text{: } L_r^* = -0.0732 + 0.0563\ \mathrm{Re}\,. \tag{15}$$

This equation is also presented in Fig. 6a. Similarly to Eq. (15) for the square cylinder with no inclination angle, a curve fit of the present inclined square cylinder results leads to

$$\text{For } \beta = 1/8:\ L_r^* = -0.604 + 0.072\ \text{Re}\ , \tag{16}$$

$$\text{For } \beta = 1/6:\ L_r^* = -0.517 + 0.061\ \text{Re}\ , \tag{17}$$

$$\text{For } \beta = 1/4:\ L_r^* = -0.527 + 0.047\ \text{Re}\ . \tag{18}$$

Deviation of each of these expressions from the computed results increases with decreasing Reynolds number. Obtaining the small values of L_r at low Re numbers is usually accompanied by the appearance of more errors in comparison with the large values of L_r. Therefore, for computing the average deviations, these maximum deviations of the computed recirculation length are neglected for each blockage ratio. The average deviations of 1.6%, 1.3%, and 3.7% are observed for β = 1/8, 1/6, and 1/4, respectively. According to these derived equations, the onset of separation for each blockage ratio can also be predicted (e.g., Re = 8.4 for β = 1/8). Comparing Eqs. (15) and (16) from Fig. 6a shows that the recirculation length for the square cylinder at $\alpha = 45^o$ in comparison with the square cylinder at $\alpha = 0^o$ (both for β = 1/8) is slightly shorter for Reynolds numbers below Re = 34.7 and larger for Reynolds numbers above this value.

4.4 Drag Coefficient

One of the most important parameters in studying flow around an obstacle is the drag coefficient (C_d). Figure 6b depicts the variation of this coefficient with the Reynolds number for three blockage ratios. The results given here agree with the classical inverse dependence of drag coefficient on the Reynolds number. It is also observed that the drag coefficient increases with the blockage ratio. The velocity gradients around the obstacle increase with the blockage ratio. Therefore, the shear stress and the viscous drag coefficient of the cylinder are also increased. On the other hand, in this situation, the head loss and the pressure drag coefficient are also increased. Increase in the individual drag coefficients lead to an increase in the total drag coefficient. Furthermore, the effect of β on C_d decreases with increasing Re. For example, increasing the blockage ratio from β = 1/8 to β = 1/4 increases the C_d by 86% for Re = 1, while this increment for Re = 40 is about 28%. Simple correlations for the total drag coefficients are found for the Reynolds numbers $1 \le \text{Re} \le 40$:

$$\text{For } \beta = 1/8:\ C_d = 1.24 + 17.84\ \text{Re}^{-1.01}\ , \tag{19}$$

$$\text{For } \beta = 1/6:\ C_d = 1.28 + 22.41\ \text{Re}^{-1.03}\ , \tag{20}$$

$$\text{For } \beta = 1/4:\ C_d = 1.32 + 34.15\ \text{Re}^{-1.05}\ . \tag{21}$$

Maximum deviations of 4%, 3.5%, and 1.2% are observed for blockage ratios of 1/8, 1/6, and 1/4, respectively.

4.5 Local Pressure Drop

Before analyzing the heat transfer results, it is worthwhile to make some comments on pressure drop in a channel. A heat transfer increment is generally accompanied by a pressure penalty. Figure 6c shows the variation of the dimensionless local pressure drop ($\Delta P^*_{cyl.}$) with the Reynolds number for different blockage ratios. As expected, a pressure drop is larger for larger blockage ratios for a fixed Reynolds number. Further data analysis shows that the effect of β on $\Delta P^*_{cyl.}$ decreases on increase in the Reynolds number for $1 \le Re \le 5$ and then increases for $10 \le Re \le 40$. However, the effect of β on $\Delta P^*_{cyl.}$ has a weak dependence on Re. Furthermore, the effects of β on $\Delta P^*_{cyl.}$ are greater than its effects on C_d. The blockage increments from $\beta = 1/8$ and $\beta = 1/6$ to $\beta = 1/4$ at Re = 40 increase $\Delta P^*_{cyl.}$ by 87% and 48%, while these blockage increments increase C_d by 28% and 19%, respectively. This can be explained by the fact that $\Delta P^*_{cyl.}$ [according to its definition in Eq. (8)] considers an additional term of the pressure drop due to the pressing of the cylinder on the channel walls. Simple correlations for the nondimensional local pressure drop are also found for the Reynolds numbers $1 \le Re \le 40$:

$$\text{For } \beta = 1/8\text{:}\ \Delta P_{cyl.}{}^{*} = 0.1252 + 1.6554\ Re^{-1.0221} \tag{22}$$

$$\text{For } \beta = 1/6\text{:}\ \Delta P_{cyl.}{}^{*} = 0.1602 + 2.7576\ Re^{-1.0306} \tag{23}$$

$$\text{For } \beta = 1/4\text{:}\ \Delta P_{cyl.}{}^{*} = 0.2436 + 6.2322\ Re^{-1.0478} \tag{24}$$

Maximum deviations of 4.7%, 4%, and 2.6% and average deviations of 1.67%, 1.42%, and 0.89% are observed for blockage ratios of 1/8, 1/6, and 1/4, respectively.

4.6 Isotherm Patterns

Isotherm patterns can provide a detailed knowledge of the temperature field that can be vital especially in continuous thermal treatment of food particles. Figure 7 shows representative isothermal profiles around the cylinder for Re = 1 and 40 each for Pr = 0.7 and 100 at two blockage ratios $\beta = 1/8$ and 1/4.

The solid lines and the dashed lines show the isotherms for the CWT and UHF conditions, respectively. Generally, it is observed that the front surfaces of the cylinder have the maximum clustering of isotherms. The crowding of isotherms clearly indicates high temperature gradients and thus relatively high values of the local Nusselt number, and vice versa. Increasing the Reynolds number for a particular value of the Prandtl number increases the temperature gradient around the obstacle due to the decrease in the momentum and in the thermal boundary layer thickness. In Fig. 7, it is also seen that for a higher Reynolds number (Re = 40) the isotherms at the back

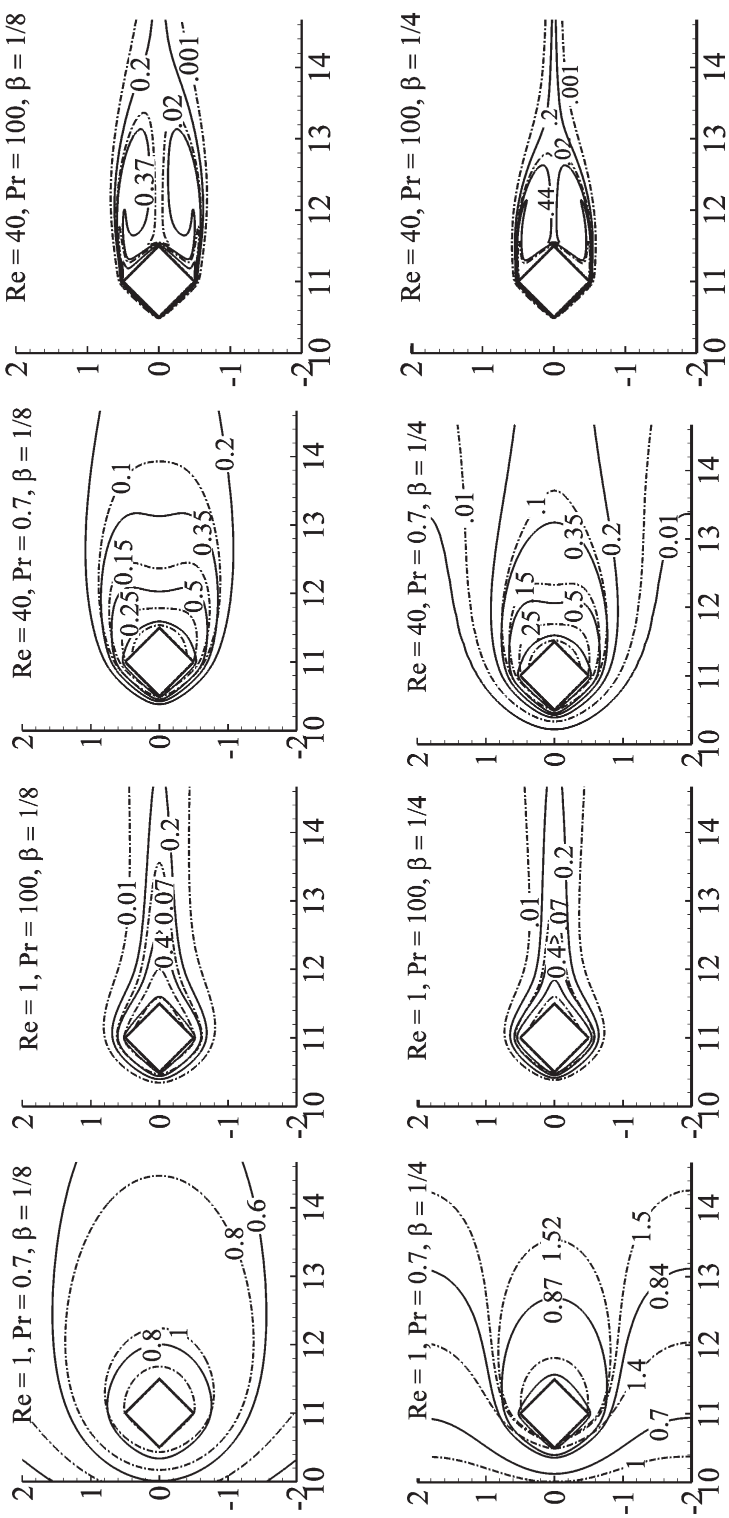

FIG. 7: Isotherms around the cylinder at different values of Re, Pr, and β for both CWT (solid lines) and UHF (dashed lines) cases

of the cylinder twist due to the existence of vortices as though the energy is bound inside them. Moreover, as the Prandtl number increases for particular Re and β, the thermal boundary layer becomes thinner and thus the crowding of isotherms around the cylinder increases. Besides, the adiabatic condition on the channel walls causes the isotherms to be distorted near the walls. As the blockage ratio increases, the effect of these distortions of isotherms approaches the cylinder. Furthermore, both CWT and UHF boundary conditions show similar tendency to changes with Re, Pr, and β. However, the UHF condition shows higher temperature gradients near the cylinder, e.g., for Re = 1, Pr = 0.7, β = 1/8 the reduction in the isotherms from 0.8 to 0.6 and from 1 to 0.8 is seen for the CWT and UHF conditions, respectively.

4.7 Local Nusselt Number

The effects of blockage ratios and Prandtl numbers on the variation of the local Nusselt number on the top surfaces of the cylinder (the flow and heat transfer on the bottom surfaces are symmetrical) at Re = 1 and 40 for UHF and CWT cases are shown in Fig. 8. Qualitatively similar features in the UHF and CWT conditions are seen in

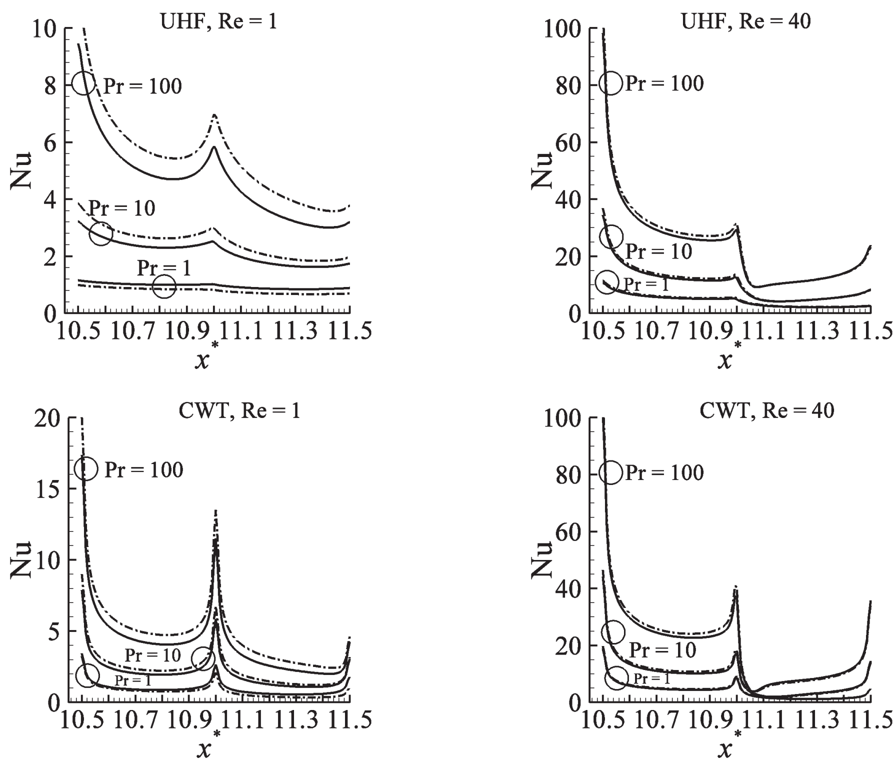

FIG. 8: Local Nusselt number variations along the cylinder top surfaces for Re = 1, 40 and Pr = 1, 10, 100 for both UHF and CWT cases at: β = 1/8 (solid lines) and β = 1/4 (dashed lines)

this figure. As expected, the local Nusselt number increases with the Reynolds number and/or Prandtl number for a fixed blockage ratio.

As the corners can be assumed to be the beginning points of the thermal boundary layers, a sharp increase in the Nu is observed at each corner of the cylinder due to the large temperature gradients normal to the surface of the obstacle. On each surface of the cylinder, Nu has a local minimum. With increasing Re, this minimum on the rear surface approaches the top edge because of the changes in the mechanisms of heat transfer by the stronger vortices. In Fig. 8 the variation of Nu is shown for $\beta = 1/8$ and 1/4. It is seen that increasing the blockage ratio leads to an increase in Nu only for larger Pr. At Re = 40, the blockage ratio has more effects on Nu on the front surface of the cylinder.

4.8 Average Nusselt Number

The average Nusselt number can be used in process engineering design calculations to estimate the rate of heat transfer from a cylinder for the CWT, or to estimate the averaged surface temperature of the cylinder for UHF. Figure 9 shows the variations of the overall average Nusselt number with the Reynolds number for both thermal boundary conditions. These figures confirm the higher average Nusselt number for the

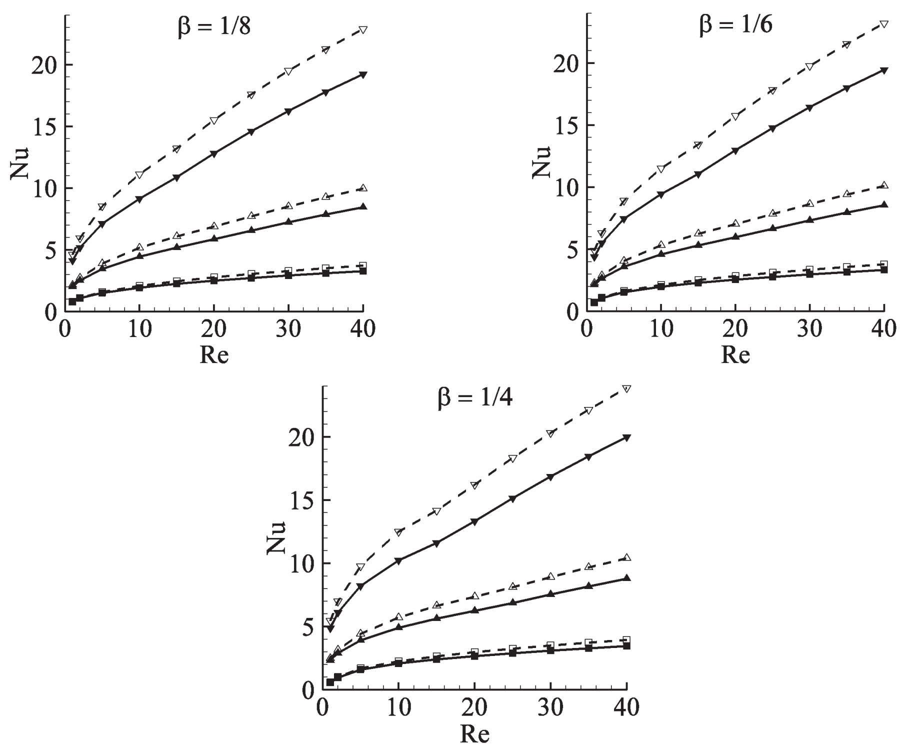

FIG. 9: Average Nu number vs. Re number for different β and Pr: (■) Pr = 0.7, (▲) Pr = 10, and (▼) Pr = 100 for CWT (filled symbols) and UHF (empty symbols) cases

UHF conditions than that for the CWT conditions. The data in this figure are close to each other and just the general behavior can be seen. The authors did a detailed analysis of the data. For example, at Re = 30, the average values of Nu for $\beta = 1/8$, 1/6, and 1/4 for CWT and Pr = 100 are 16.8577, 16.4465, and 16.2538, respectively. Decreasing the blockage ratio increases the average Nusselt number at low Re and Pr numbers (Re = 1, 2 and Pr = 0.7, 1). For example, decreasing β from $\beta = 1/4$ to $\beta = 1/8$ increases the Nu by 38% and 25% at Re = 1 in the CWT conditions for Pr = 0.7 and 1, respectively. However, for other Re and Pr numbers the average Nu numbers increase with the blockage ratios. Generally, the increases in the Nusselt number with the blockage ratios are greater at low Reynolds numbers and in the UHF conditions. The maximum increase in the Nusselt number with the blockage ratio is about 18.3% for blockage increment from $\beta = 1/8$ to $\beta = 1/4$ at Re = 1 and Pr = 100 in the UHF conditions.

Correlating the present heat transfer results by simple expressions is useful and convenient for engineering applications. Further data analysis exhibits the classical dependence of the Nusselt number on Prandtl number, i.e., $Nu \alpha Pr^{1/3}$. So, the important parameter for process engineering design calculations, the Colburn *j*-factor ($j = Nu/(Re\, Pr^{1/3})$), is usable here. The Colburn *j*-factor is represented as a function of Re in Fig. 10. The best nonlinear curve fittings for all the results presented in Fig. 10

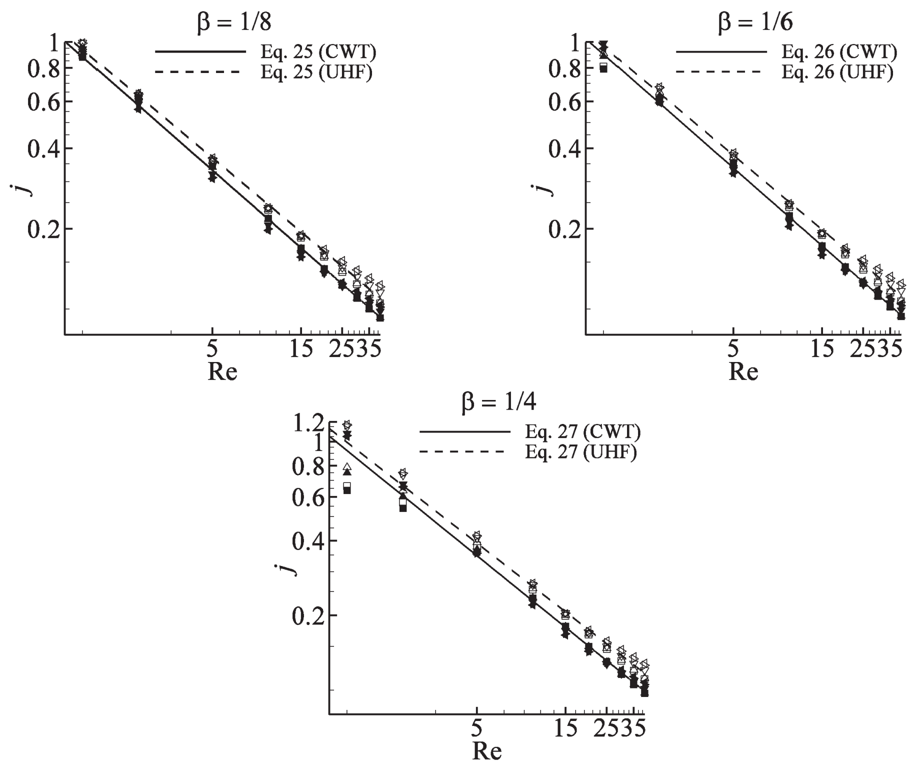

FIG. 10: The Colburn *j* factor vs, Re at different β for CWT (filled symbols) and UHF (empty symbols) in different Pr: (■) Pr = 0.7, (▲) Pr = 1, (▼) Pr = 10,(►) Pr = 50, (◄) Pr = 100

for both boundary conditions within the ranges $1 \le \mathrm{Re} \le 40$ and $0.7 \le \mathrm{Pr} \le 100$ give the following correlations:

$$\text{For } \beta = 1/8, \text{CWT: } j = 0.8841 \ \mathrm{Re}^{-0.6102} \ \& \ \text{UHF: } j = 0.9411 \ \mathrm{Re}^{-0.5823}, \quad (25)$$

$$\text{For } \beta = 1/6, \text{CWT: } j = 0.9022 \ \mathrm{Re}^{-0.6109} \ \& \ \text{UHF: } j = 0.9643 \ \mathrm{Re}^{-0.5839}, \quad (26)$$

$$\text{For } \beta = 1/4, \text{CWT: } j = 0.9207 \ \mathrm{Re}^{-0.6044} \ \& \ \text{UHF: } j = 0.9940 \ \mathrm{Re}^{-0.5797}. \quad (27)$$

The expressions for the CWT conditions have maximum deviations of 10%, 9%, and 8% for β = 1/8, 1/6, and 1/4, respectively, and the average deviation of about 3% for all blockage ratios. The maximum and average deviations for the UHF conditions are also about 9% and 4% for all blockage ratios. It should be noted here that almost all deviations for drag coefficient, local pressure drop, and the average Nusselt number increase with a decreasing blockage ratio. This can be explained by the developments of the instabilities and irregularities in the flow domain due to the decreasing blockage ratio, so the data distributions occur in a larger domain and the deviations increase.

Further attention to these correlations can give good results. For example, it can be concluded that the dependence of Nu on Pr increases with the blockage ratio as the constants of the correlations increase with blockage. The dependence of the average Nu number on the third root of the Pr number ($\mathrm{Nu} \alpha \mathrm{Pr}^{1/3}$) also shows that from the viewpoint of engineering application, the constant thermo-physical properties are not a poor assumption. Even a 100% growth in the Pr value will change the Nu only by 26%.

5. CONCLUSIONS

A lack of accurate and detailed data was found in the literature for steady flow and heat transfer around a confined inclined square cylinder that initiated the present work. In this study, the effects of the blockage ratio and Prandtl number on the flow and heat transfer characteristics of Newtonian fluids across an inclined square cylinder were investigated for a wide range of Prandtl numbers ($0.7 \le \mathrm{Pr} \le 100$) and three different blockage ratios (β = 1/8, 1/6, and 1/4) in a steady flow regime ($1 \le \mathrm{Re} \le 40$). The effects of two types of thermal boundary conditions (CWT and UHF) on the Nusselt number were studied. Generally, the use of the UHF boundary conditions yields slightly higher values of the Nusselt number. The streamlines and isotherms around the obstacle are presented. It is observed that the flow separation starts from the cylinder rear surface in the range $5 \le \mathrm{Re} \le 15$ for three blockage ratios. The length of the recirculation zone is also seen to decrease with an increasing blockage ratio. Generally, decreasing the blockage ratio decreases the dimensionless local pressure drop for the cylinder. Furthermore, for low Re and Pr numbers (Re = 1, 2 and Pr = 0.7, 1), a decreasing blockage ratio increases the average Nusselt number. For example, decreasing β from β = 1/4 to β = 1/8 increases the Nu by 38% and decreases the

$\Delta P^*_{\text{cyl.}}$ by 46% at Re = 1 for Pr = 0.7 in the CWT conditions. Therefore, decreasing the blockage ratio for low Reynolds and Prandtl numbers can be an economical way for improving the thermal efficiency of the problem. However, for larger Reynolds and Prandtl numbers the average Nusselt number increases with the blockage ratio. For example, for Re = 1 and Pr = 100 in the UHF conditions, the blockage increment from $\beta = 1/8$ to $\beta = 1/4$ increases the Nu and $\Delta P^*_{\text{cyl.}}$ by 18.3% and 46%, respectively. Finally, simple correlations for L^*_{r}, C_{d}, $\Delta P^*_{\text{cyl.}}$, and Nu (in terms of the Colburn *j*-factor) were obtained for different blockage ratios over the range of physical parameters considered in this study.

REFERENCES

Aboueian-Jahromi, J., Hossein Nezhad, A., and Behzadmehr, A., Effects of inclination angle on the steady flow and heat transfer of power-law fluids around a heated inclined square cylinder in a plane channel, *J. Non-Newtonian Fluid Mech.*, vol. **166**, pp. 1406–1414, 2011.

Ahmad, R. A., Steady-state numerical solution of the Navier–Stokes and energy equations around a horizontal cylinder at moderate Reynolds numbers from 100 to 500, *Heat Transfer Eng.*, vol. **17**, pp. 31–81, 1996.

Benim, A. C., Aslan, E., and Taymaz, I., Lattice Boltzmann method for laminar forced convection in a channel with a triangular prism, *Heat Transfer Res.*, vol. **42**, no. 4, pp. 359–377, 2011.

Bharti, R. P., Chhabra, R. P., and Eswaran, V., A numerical study of the steady forced convection heat transfer from an unconfined circular cylinder, *Heat Mass Transfer*, vol. **43**, pp. 639–648, 2007.

Breuer, M., Bernsdorf, J., Zeiser, T., and Durst, F., Accurate computations of the laminar flow past a square cylinder based on two different methods: lattice-Boltzmann and finite-volume, *Int. J. Heat Fluid Flow*, vol. **21**, pp. 186–196, 2000.

Chakrabarty, D. and Brahma, R., Effect of wall proximity in fluid flow and heat transfer from a square prism placed inside a wind tunnel, *Thermal Sci.*, vol. **11**, no. 4, pp. 65–78, 2007.

Chhabra, R. P. and Richardson, J. F., *Non-Newtonian Flow and Applied Rheology*, 2nd ed., Oxford, U.K: Butterworth-Heinemann, 2008.

Coelho, P. M. and Pinho, F. T., A generalized Brinkman number for non-Newtonian duct flows, *J. Non-Newtonian Fluid Mech.*, vol. **156**, pp. 202–206, 2009.

Davis, R. W., Moore, E. F., and Purtell, L. P., A numerical-experimental study of confined flow around rectangular cylinders, *Phys. Fluids*, vol. **27**, pp. 46–59, 1984.

Dhiman, A. K., Chhabra, R. P., and Eswaran, V., Flow and heat transfer across a confined square cylinder in the steady flow regime: effect of Peclet number, *Int. J. Heat Mass Transfer*, vol. **48**, pp. 4598–4514, 2005.

Dhiman, A. K., Chhabra, R. P., Sharma, A., and Eswaran, V., Effects of Reynolds and Prandtl numbers on the heat transfer across a square cylinder in the steady flow regime, *Numer. Heat Transfer, Part A*, vol. **49**, pp. 717–731, 2006.

Gupta, A. K., Sharma, A., Chhabra, R. P., and Eswaran, V., Two-dimensional steady flow of a power law fluid past a square cylinder in a plane channel: momentum and heat transfer characteristics, *Ind. Eng. Chem. Res.*, vol. **42**, pp. 5674–5686, 2003.

Igarashi, T., Characteristics of the flow around a square prism, *Bull. JSME*, vol. **27**, pp. 1858–1865, 1984.

Moussaoui, M. A., Jami, M., Mezrhab, A., and Naji, H., MRT-lattice Boltzmann simulation of forced convection in a plane channel with an inclined square cylinder, *Int. J. Thermal Sci.*, vol. **49**, pp. 131–142, 2010.

Sahu, A. K., Chhabra, R. P., and Eswaran, V., Effects of Reynolds and Prandtl numbers on heat transfer from a square cylinder in the unsteady flow regime. *Int. J. Heat Mass Transfer*, vol. **52**, pp. 839–850, 2009.

Sharma, A. and Eswaran, V., Heat and fluid flow across a square cylinder in the two-dimensional laminar flow regime, *Numer. Heat Transfer, Part A*, vol. **45**, pp. 247–269, 2004.

Sohankar, A., Norberg, C., and Davidson, L., Low Reynolds number flow around a square cylinder at incidence: study of blockage, onset of vortex shedding and outlet boundary condition, *Int. J. Numer. Meth. Fluids*, vol. **26**, pp. 39–56, 1998.

Turki, S., Abbassi, H., and Nasrallah, S. B., Two-dimensional laminar fluid flow and heat transfer in a channel with a built-in heated square cylinder, *Int. J. Thermal Sci.*, vol. **42**, pp. 1105–1113, 2003.

Valencia, A., Heat transfer enhancement in a channel with a built-in square cylinder, *Int. Commun. Heat Mass Transfer*, vol. **22**, no. 1, pp. 47–58, 1995.

Yoon, D. H., Yang, K. S., and Choi, C. B., Heat transfer enhancement in channel flow using an inclined square cylinder, *J. Heat Transfer*, vol. **131**, pp. 745031–745034, 2009.

Yoon, D. H., Yang, K. S., and Choi, C. B., Flow past a square cylinder with an angle of incidence, *Phys. Fluids*, vol. **22**, pp. 436031–4360312, 2010.

Zdravkovich, M. M., *Flow around Circular Cylinders: Fundamentals,* vol. 1, New York: Oxford University Press, 1997.

Zdravkovich, M. M., *Flow around Circular Cylinders: Applications,* vol. 2, New York: Oxford University Press, 2003.